ACS Catalysis

Research Article

pubs.acs.org/acscatalysis

A Study of Pt Dissolution during Formic Acid Oxidation

M. Fayette,[†] J. Nutariya,[‡] N. Vasiljevic,*[,‡] and N. Dimitrov*[,†]

[†]Department of Chemistry, SUNY at Binghamton, Binghamton, New York 13902, United States

[‡]School of Physics, H.H. Wills Physics Laboratory, University of Bristol, Bristol BS8 1TL, U.K.

Supporting Information

ABSTRACT: The studies on Pt or Pt-alloy based catalysts for formic acid oxidation (FAO) have been focused mostly on their activity with little analysis of durability and long-term performance. While durability of Pt-based FAO catalysts has been associated with CO poisoning, recent studies have brought evidence of correlation between catalyst performance and dissolution of Pt. Aimed at assessing the impact of that correlation, a detailed quantitative durability analysis of Pt ultrathin films grown on Au by surface limited redox replacement of a Pb underpotentially deposited layer is presented in this work. Long-term catalytic performance of those films featuring well-defined thickness and structure has been examined by potential cycling in 2 M HCOOH+0.1 M $HClO_4$ solution at sweep rate of 0.050 V s^{-1} over an extended potential range limited positively by the onset of Pt oxidation. A clear proportionality between overall life and thickness of the catalyst observed in the tests emphasizes the dissolution of Pt as the key life-limiting factor. The steady loss of Pt during cycling has been also confirmed by XPS compositional analysis. Ex situ imaging, performed by SEM and AFM at characteristic stages of the activity decay (associated with distinctive voltammetric behavior), reveals dramatic morphological changes accompanying the Pt dissolution process. An average Pt dissolution rate of 272 ± 30 ng·cm^{-2}·h^{-1} has been determined based on the FAO activity decay of Pt films of different thickness. For comparison, identical experiments performed in the absence of formic acid showed about 4−5 times lower Pt dissolution rate, in the range of 61 ± 8 ng·cm^{-2}·h^{-1}. The significant impact of the FAO on the dissolution rate suggests a possibility of reaction intermediate contribution to the dissolution of Pt.

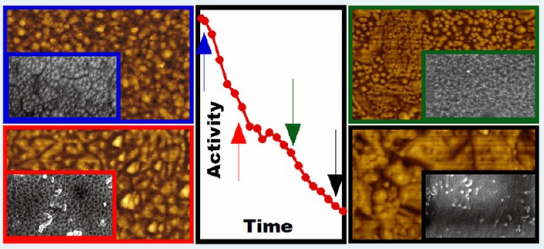

KEYWORDS: *formic acid oxidation, Pt catalyst, Pt dissolution, Pt oxidation, Pt durability, CO poisoning*

INTRODUCTION

In the past few decades, the development of polymer electrolyte membrane fuel cells (PEMFC) as powerful sources of "green" energy attracted significant attention.[1−3] The scientific and technological focus has been on the development of highly active yet durable Pt-based catalysts for both cathodic[4−8] (oxygen reduction reaction, ORR) and anodic fuel cell reactions[9−19] (hydrogen/hydrocarbon oxidation). PEMFC using formic acid as a fuel (direct formic acid fuel cell, DFAFC) has been considered a viable option for portable power devices.[2,20]

Comprehensive studies of *formic acid oxidation* (FAO) on Pt performed decades ago proposed a dual-pathway mechanism[21−23] that involves (1) dehydrogenation of formic acid, which produces CO_2 via one or more reactive intermediates (*direct path*) and (2) dehydration of formic acid with the formation of CO_{ad} acting as the "poisoning" or reactive intermediate (*indirect path*).[21,23−26] Since then, most of the work in this field has been focused on the development of active and durable bimetallic catalysts for FAO reaction such as the state-of-the-art Pt[11,27−29] overlayers or Pt alloys (PtRu,[10] PtCu,[16,17] PtPb,[14,30,31] PtPd,[12] PtBi,[15,19,31] etc.) that would either promote the "direct pathway" or minimize the poisoning associated with the "indirect" one. Designed in the form of nanoparticles or ultrathin films these systems address the challenges of Pt limited supply and the related catalysts' high price. In recent time, emphasis has been placed on the maximum performance of bimetallic catalysts and especially on the enhanced activity attributed to bifunctional, ensemble, or electronic effects.[10,32] In the longer term, the mechanism of FAO on Pt has been explored for decades, but debates on fundamental aspects of both mechanistic details on the molecular level and the actual nature of reactive intermediates are still ongoing.[22,33−39] The nature of the reactive intermediates in the direct pathway has been particularly controversial, as clearly seen through the discussion revolving around works of Osawa et al.,[37,40] Behm et al.,[35,38,39] and Cuesta et al.[36] This controversy not only illustrates the FAO mechanism complexity but also reveals its strong dependence on the applied potential and on the presence of reactive intermediates or coasdorbate species.

The focus on FAO mechanism and the ever existing drive to Pt-based catalysts with higher activity have left very little attention on the catalysts' durability during FAO and related fundamental aspects of Pt dissolution. The thus far limited number of FAO studies on Pt and Pt-alloys have partially

Received: January 10, 2013
Revised: June 23, 2013
Published: June 24, 2013

examined durability conducted either potentiostatically (over short time, 10−30 min)[17,30] or potentiodynamically, employing pulsing[41] or cycling protocols.[16,31,42,43] The constant potential testing was generally focused on and somewhat limited by the low potential CO_{ad} poisoning that rapidly reduces catalytic activity.[17,30] The potentiodynamic testing better reflects the complexity of fuel cell operation,[44] but its power in controlling the effect of CO_{ad} poisoning/reacting depends substantially upon the choice of potential limits. Thus, a high positive potential limit would favor oxygen adsorption/surface oxidation leading to CO_{ad} oxidation and its removal from the catalyst's surface.[21,45] In support of the latter scenario, a recent work of ours demonstrated that choice of positive potential limit in the range 1.3−1.4 V (NHE) marginalizes the effect of CO_{ad} poisoning in FAO durability tests carried out by potential cycling on bulk Pt.[43] Another important finding of durability testing of Pt-based catalysts (Pt and PtCu alloys) has been the strong impact of Pt dissolution on the lifetime of catalysts with limited Pt content (thin films and nanoparticles).[16,42,43] These results not only identify the dissolution of Pt as a key factor impacting the catalysts' durability but also point toward a delicate balance between (i) Pt dissolution and (ii) interplay between FAO intermediate adsorption, CO_{ad} poisoning, and Pt oxidation in the course of potential cycling.[43] No extra fundamental insight on catalysts' durability in FAO is available because most of the Pt dissolution oriented research has been performed through the prism of PEMFC development with focus on the ORR in perchlorate or sulfate acidic solutions. More specifically, several recent reviews on PEMFC Pt nanoscale catalysts[44,46,47] emphasize as areas of interest: (i) the degradation of Pt nanoparticles supported on carbon associated with dissolution of carbon support,[46,48] (ii) Pt solubility along with mechanism of Pt dissolution under both equilibrium and nonequilibrium conditions,[44] and (iii) Pt and Pt-alloy nanoparticle degradation under different polarization and cycling conditions.[48−50] However, despite some recent advances, the mechanistic understanding of the dissolution process even on a planar Pt surface in background electrolyte is still incomplete. It is unclear whether Pt dissolution is an anodic process taking place alongside Pt oxidation or a cathodic one happening during oxide−reduction and facilitated by chemical dissolution of Pt-oxide.[51−55] In both cases, Pt-oxide species seem to be a key contributor to the dissolution processes. Supporting that claim, most recent ICP-MS studies of Mayrhofer et al.[55] provide clear evidence for strong impact of operation conditions like cycling, polarization, pH, etc. (all controlling the Pt oxide formation), on Pt dissolution in perchloric acid solutions. Other fundamental studies of bulk Pt dissolution have been performed also in background electrolytes using potential cycling (often referred to as electrochemical activation)[51,52,55−59] and potentiostatic conditions[60,61] Higher dissolution rates have been reported for the potential cycling experiments.[56,60] Also the effect of acidic media on the dissolution of Pt has been assessed in early work of Johnson et al.,[51] Rand et al.,[56] and Kinoshita et al,[57] in sulfuric (1 M H_2SO_4) and perchloric (0.1 M $HClO_4$) background electrolytes. Points of interest in these studies have been effect of the negative potential limit, the Pt surface area evolution during dissolution, and the nature of the dissolved Pt complex. Pt dissolution rates of 2.0−5.5 ng·cm^{-2} per cycle have been reported for various sweep rates during potential cycling with negative potential limit between 1.2 and 1.5 V (NHE).[51,56−58] So far it has been found that in perchloric acid media the primary dissolution product is a Pt(II)[47,52] complex whereas in sulfuric acid a Pt(IV) complex dominates among the oxidized species.[51,56] Recent *in situ* work of Komanicky et al. has demonstrated an effect of the crystallographic orientation on Pt dissolution in 0.6 M $HClO_4$ at constant potentials by identifying the (111) facets as being more prone to dissolution than the (100).[61]

To the best of our knowledge, no quantitative investigation of Pt dissolution has been performed so far during electrooxidation of formic acid. Few studies, among them the work of Zhang et al.,[62] where formic acid is used as a contaminant, and recent work of ours,[16,43] have associated the dissolution of Pt with trends in the performance and durability of the catalyst. More specifically, a comparison of oriented Pt and PtCu nanoparticles[16,43] with their planar thin film counterparts has revealed a correlation between the loss of catalytic activity and catalyst dissolution. Building upon these findings, we present here the first multifaceted and detailed quantitative study of Pt dissolution during FAO. Technically, the study is conducted on Pt thin films grown on Au by surface limited redox replacement (SLRR) of Pb underpotentially deposited (UPD) layers.[28] Developed recently, the SLRR deposition approach provides remarkable control of structure and thickness of epitaxially deposited Pt films. This along with knowledge on the characteristic voltammetric behavior changes correlated with Pt dissolution during FAO enable quantitative Pt loss measurements. The testing is limited to Pt ultrathin layers of preselected thickness deposited on bulk polycrystalline Au and (111) textured Au thin films. The loss of Pt is studied under cycling conditions with the positive potential limit set at the onset of Pt oxidation, which allows for minimization of the CO_{ad} poisoning effect and enables comparisons with previously reported results.[16,42,43] The characterization of Pt catalyst at different stages of dissolution have been conducted by X-ray photoelectron spectroscopy (XPS) analysis and cyclic voltammetry (CV), that is, H UPD. The Pt dissolution kinetics has been studied through the activity loss during FAO monitored by CV. The corresponding morphological changes have been documented by scanning electron microscopy (SEM) and ex-situ atomic force microscopy (AFM) imaging.

EXPERIMENTAL SECTION

Preparation of Au and Pt Polycrystalline Electrodes. Polycrystalline Au and Pt disks, d = 0.6 cm, 2 mm thick, were used as working electrodes (WE) in this study along with the Au thin films grown on Si wafers. Au and Pt crystals were initially mechanically polished down to 0.05 μm using water-based, deagglomerated alumina suspensions (Buehler) followed by electropolishing by dc anodization in 30:7:5 ethylene glycol, hydrochloric acid, and glacial acetic acid using Ag wire as a cathode. Au samples were treated for 10−15 s at dc current density of ∼2.5 A cm^{-2}, while Pt samples were treated by anodization of ten impulses of 1 s at the same current density. After the electropolishing step, both Au and Pt samples were immersed in concentrated HNO_3 to remove any remnants of the polishing runs followed by thorough rinsing with Barnstead Nanopure water (>18 MΩ cm). Prior to experiments, the crystals were annealed until "red-hot" with a propane torch and then cooled under N_2 atmosphere. After annealing, a water droplet was placed upon the electrode surface to prevent contamination, and then the electrode was immersed in a three-electrode cell in a "hanging meniscus" configuration.

Preparation of Au Thin Film Electrodes. The Au thin films 250 nm thick were ultrahigh vapor deposited on Si-wafers with a 4 nm Ti adhesion layer. The X-ray diffraction θ−2θ measurements showed (111) texture with average grain size of 30 nm. The Au films were cleaned in concentrated HNO_3 and H_2SO_4 followed by rinsing by

dx.doi.org/10.1021/cs400347u | ACS Catal. 2013, 3, 1709−1718

Barnsted Nanopure water and drying in pure N_2. All Au films were flame annealed using a propane torch under constant N_2 flow in a Purex tube with the flame directed outside the tube for 1−2 min. The annealing protocol resulted in reproducible Au (111) textured films featuring average grain size of 100−200 nm.

Pt Ultrathin Film Deposition. The growth of Pt films on Au film has been conducted by SLRR of Pb UPD in one cell configuration as described in detail in previous work.[28] Growth solution 0.1 M $NaClO_4$ (Sigma, 99.95%), 1 mM $HClO_4$ (GFS Chemical, 70% redistilled), 1 mM $Pb(ClO_4)_2$ (Aldrich, 99.995%), and 0.5 mM $K_2(PtCl_4)$ (Sigma Aldrich 99.999%) was thoroughly deoxygenated by purging with ultrahigh purity N_2 for 2 h. SLRR cycles consisted of repeated metal UPD formation steps (one-second potential impulse at −0.83 V) followed by redox replacement of a UPD layer by Pt (at open circuit). The deposition was controlled and monitored using an OMNI 90 (Cypress Systems) potentiostat coupled to a PC using a Cypress Systems electronics module and analog-to-digital converting board "National Instruments". Dasylab software (version 9.00) was used to operate and control the setup.

Electrochemical Testing and Characterization. The quality of deposited Pt films was characterized by H UPD conducted by cyclic voltammetry in 0.5 M H_2SO_4 (GFS Chemical, highest purity grade, redistilled). FAO experiments were conducted by cyclic voltametry in solution containing 0.1 M $HClO_4$ and 2 M HCOOH (Sigma, 98%) at sweep rate of 0.050 V s^{-1} in the potential range −0.500 to 0.800 V. Control experiments were carried out using the same cyclic conditions (potential limits and sweep rate) in solution containing 0.1 M $HClO_4$. The characterization of Pt films was performed using model AFCBP bipotentiostat (Pine Instruments) interfaced with a PC through the Pinechem software (Version 2.80). All solutions were made using Barnsted Nanopure water and high-purity grade chemicals as received from the vendors. Unless stated otherwise, a saturated mercury−mercurous sulfate electrode (MSE) was used as reference electrode and Pt wire as counter electrode. All potentials in the manuscript are presented versus MSE, and all current densities present normalization of the current with respect to the geometric area of the electrode.

Ex Situ Surface Characterization. AFM characterization of Pt surface morphology at different stages of prolonged FAO was performed ex situ in tapping mode, right after the electrochemical characterization in 0.5 M H_2SO_4. The AFM study has been conducted using Dimension 3000 Veeco AFM system with NanoScope V SPM controller. XPS characterization of Pt films grown by 30 SLRR events was performed on a PHI 5000 Versaprobe from Physical Electronics with monochromatic Al Kα X-rays (1486.6 eV). The spot size was 100 μm × 1400 μm X-ray at 100 W with pass energy of 187.75 eV for survey scans (0−1400 eV) and 23.5 eV for region spectra. The take off angle was 45°. Depth profiling measurements were done using sputtered Ar^+ at a rate of 0.5 kV/min. SEM images were obtained using a FE-SEM Supra 55VP with EHT = 10.00 kV and a working distance of 3.2 mm.

RESULTS AND DISCUSSION

Demonstration of Pt Dissolution during HCOOH Oxidation. The dissolution of Pt at positive potentials and during potential cycling in background electrolytes so far had been mainly measured and detected by analytical approaches based on the solution elemental analysis.[56,57,60,61] For example, the variety of atomic spectroscopy (absorption, colorimetry, mass spectroscopy), rotating disk electrode technique,[51] and most recently ICP-MS[55] have been employed to (i) prove the presence of dissolved Pt and (ii) decouple between Pt(II) and Pt(IV) complexes formed during dissolution.

Our recent study in 2 M HCOOH + 0.1 M $HClO_4$ solution revealed a significant difference in the long term behavior of bulk Pt and Pt thin films deposited on Au (*hkl*).[43] A steady long-term electrochemical behavior of the former and limited life of the latter[43] suggested Pt dissolution as a likely reason for this significant difference. To start, we employed an electrochemically based approach to demonstrate that Pt dissolution takes place during the course of FAO potential cycling by detecting the presence of dissolved Pt complex in the solution. The approach is based on use of Au counter electrode (CE), which during FAO cycling can "detect" dissolved Pt species, if present in the solution, by their reduction on the CE. A markedly different electrochemical behavior of Pt and Au in sulfate solution then can be used as qualitative monitoring of the Pt dissolution process (Pt does and Au does not exhibit H UPD). Figure 1 shows the electrochemical analysis of Au electrode before and after different times of use as CE during FAO, examined in a separate cell with 0.5 M H_2SO_4 solution.

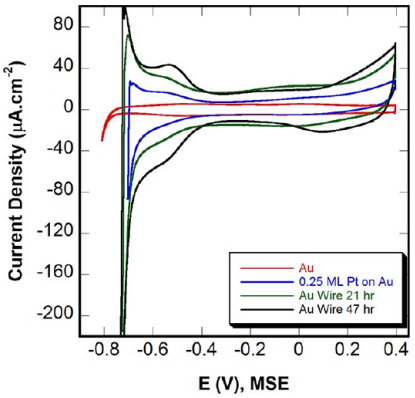

Figure 1. Cyclic voltammetry (CV) curves in 0.5 M H_2SO_4 of Au wire before (red) and after use as counter electrode (CE) in 2 M HCOOH + 0.1 M $HClO_4$ solution in which bulk Pt electrode is cycled for 21 h (green) and 47 h (black). For the sake of comparison, CV of 0.25 ML of Pt deposited on Au via SLRR is presented (blue). Scan rate 0.050 V s^{-1}.

As it can been seen in Figure 1, the pure Au electrode features typical sulfate adsorption[63] (not pronounced on presented CV) and onset of hydrogen evolution reaction (HER) at a potential of approximately −0.75 V. However, a very different voltammetric behavior is obtained on the Au wire after its use as counter electrode during cycling for 21 h in FAO testing. The onset of HER shifts about 0.12 V positively and very distinguishable shoulders, characteristic of H UPD on Pt, can be observed.[28] For the sake of comparison, voltammetry of Au wire with a submonolayer amount of Pt (~0.25 ML) deposited by SLRR is also presented. The remarkable shape similarity of both CV curves suggests a submonolayer amount of Pt deposited on the Au wire after 21 h of FAO testing. Figure 1 also shows the same Au wire serving as CE for longer FAO cycling of 47 h. The corresponding curve indicates the presence of more Pt on the CE as the H UPD charge apparently increases and the associated CV characteristics become more pronounced. The corresponding CV curve features a pronounced peak at −0.50 V indicative of predominant Pt(100) facets.[64] Also the charge measured under the H UPD peaks suggests nearly complete coverage of the Au electrode by Pt. In conclusion, while no quantitative data could be obtained by the experiment described in this section, its value is in the clear demonstration of Pt accumulation on the Au CE over long-term FAO testing of bulk Pt. That finding undoubtedly suggests a Pt dissolution process taking place at a measurable rate. Quantitative aspects of the dissolution kinetics are presented and discussed at the end of the Results and Discussion section.

dx.doi.org/10.1021/cs400347u | ACS Catal. 2013, 3, 1709−1718

Dissolution of Pt Ultrathin Films with Controlled Thickness. To gain a better understanding of the dissolution process and make a quantitative dissolution rate assessment during FAO, Pt thin films of varying thickness have been examined. The thickness control is strictly exercised by the SLRR approach for Pt deposition providing for the growth of one Pt monolayer per each replacement (R) event. In order to avoid ambiguities related to crystallographic orientation effects on the dissolution of oriented Pt faces reported in earlier work[43] (e.g., (100) face is more durable than the (111) face), we have examined FAO on Pt films grown on the Au-poly (polycrystalline) substrate with uniform and reproducible structure.[28] The electrochemical characterization by H UPD of Pt films of different thickness is shown in Figure 2. The

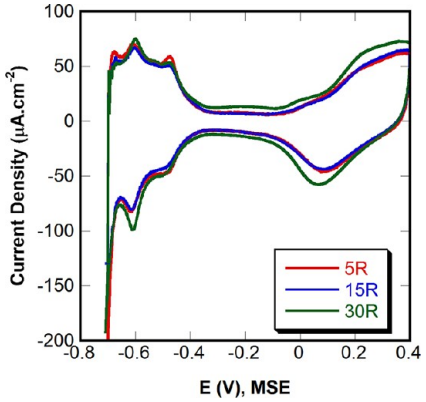

Figure 2. H UPD in 0.5 M H_2SO_4 on Pt films deposited on Au-poly after different numbers of SLRR events (*R*) using Pb UPD: 5*R* (red), 15*R* (blue), and 30*R* (green). Scan rate 0.050 V s^{-1}.

quality of Pt films of different thicknesses is in agreement with earlier reported results[28] showing no significant surface area evolution even after 30 SLRR events of growth. The films feature a roughness no greater than 1.5 based on the charge of H UPD[28,65] normalized to the monolayer charge of 210 μC cm^{-2} for atomically flat (111) surface.[66,67] Figure 3 shows the HCOOH oxidation CV curves after three cycles with 0.050 V s^{-1} scan rate on corresponding Pt films of different thickness. Apparently, all three films regardless of thickness exhibit approximately the same catalytic activity (18−20 mA cm^{-2})

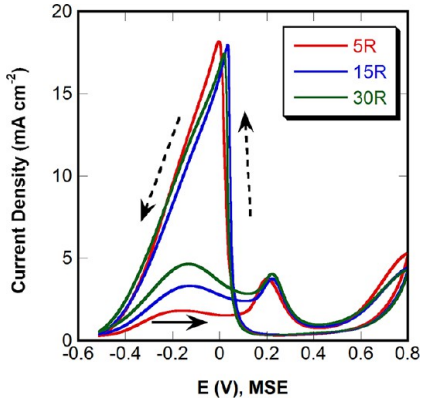

Figure 3. Cyclic voltammetry curves of formic acid oxidation on Pt films deposited on Au-poly after 5 (red),15 (blue), and 30 (green) SLRR replacement events in 2 M HCOOH + 0.1 M $HClO_4$ solution. Scan rate 0.050 V s^{-1}.

that we assign here to a maximum current density of the peak in the negative potential scan (dashed arrows) measured initially at about 0.0 V. The only noticeable difference in the voltammetry curves can be seen in the positive scan (solid arrows) peaks where the oxidative current increase follows the increase of the Pt film thickness. Such difference is not surprising knowing that ensemble and electronic effects of the Au substrate can be manifested by thickness dependent catalytic activity and by adsorption of intermediates that with increased thickness approaches bulk metal behavior.[68,69]

The activity gradually decreases during FAO cycling at constant rate of 0.050 V s^{-1}, as shown in Figure 4 where the

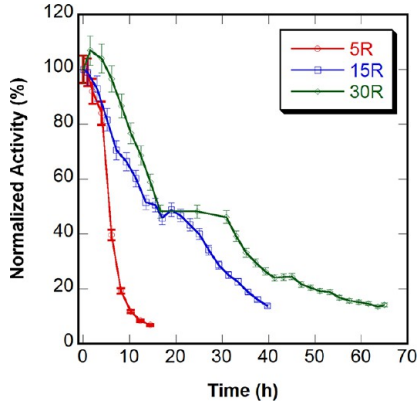

Figure 4. Normalized activity decay for Pt films deposited on Au-poly after 5 (red), 15 (blue), and 30 (green) SLRR events. Solution 2 M HCOOH + 0.1 M $HClO_4$. Scan rate 0.050 V s^{-1}.

activity of the sample is presented as normalized, relative (percentage), value of the initially measured one. The results in Figure 4 clearly demonstrate the direct correlation between the amount of Pt and catalyst durability. Considering "complete loss" of the catalyst as the time it takes the activity to drop to 20% of the initial value, it can observed that it takes about 8 h for Pt film grown by 5 SLRR events, about 30 h for 15 SLRR events, and finally about 60 h for 30 SLRR events. This suggests that the catalyst durability dependence on Pt film thickness is nearly linear. The detailed inspection of the curves in Figure 4 shows decays featuring plateaus at around 50−60% activity (very pronounced for films grown by 15 and 30 SLRR events). This trend is similar to the one reported in our recent works on crystallographically oriented Pt and PtCu nanoparticle and thin film catalysts.[43] It must be mentioned that lowering the positive cycling limit on the same Pt films leads to activity decays qualitatively similar in shape, albeit 1.5−2 times slower in reaching the 20% mark. Overall, the common trend of activity decay on Pt-based catalysts of limited thicknesses undoubtedly identifies Pt dissolution as the leading factor for loss of catalytic performance during potential cycling. This is further supported by the lack of such activity decay on bulk Pt samples reported in our earlier work, which was attributed there to the "infinite supply" of Pt.[43]

XPS Characterization. In order to obtain quantitative confirmation of Pt dissolution, films grown by 30 SLRR events on polycrystalline Au were analyzed by XPS after being subjected to different number of cycles (i.e., time) of FAO. As seen in the Figure 5, the control sample (t = 0, with no FAO cycling) shows absence of the Au substrate $4f^5$ and $4f^7$ peaks. This indicates that the Au surface is completely screened off by Pt prior to potential cycling and shows the XPS spectra

dx.doi.org/10.1021/cs400347u | ACS Catal. 2013, 3, 1709−1718

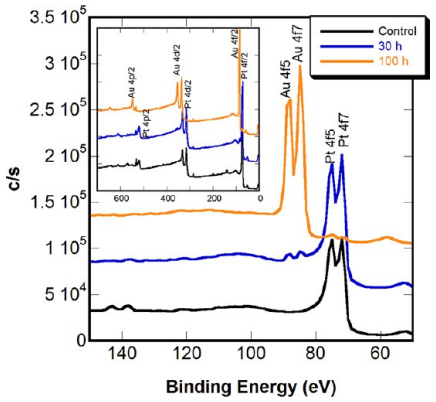

Figure 5. XPS excitation of 4f electrons recorded on Pt thin films deposited by 30 SLRR events on Au after 0 (black), 30 (blue), or 100 h (yellow) of potential cycling in 2 M HCOOH + 0.1 M $HClO_4$ with scan rate of 0.050 V s^{-1}. Inset, XPS scans of the same samples in broader binding energy range.

(especially the Pt 4f peaks) of intact Pt film. After 30 h of FAO cycling the XPS shows marginal presence of Au on the surface (see the onset of Au $4f^5$ and $4f^7$ doublet peak at 84−87 eV). However, the spectra completely changes for the sample tested by potential cycling for 100 h. In that case, clear presence of Au is evident by prominent Au $4f^5$ and $4f^7$ doublet peaks with marginal traces of Pt manifested by a hint of doublet peak of Pt $4f^5$ and $4f^7$.

The analysis is further supported by a depth-profile XPS examination of the sample before and after FAO cycling shown in Figure 6. The comparison of depth profile of the control

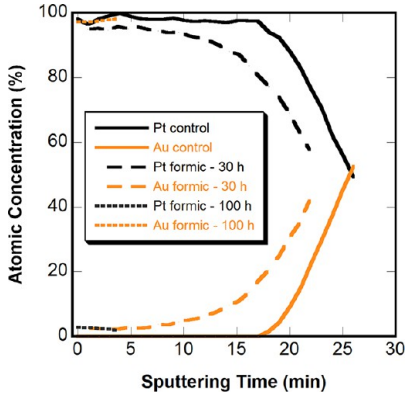

Figure 6. XPS depth-profiles of Pt thin films deposited by 30 SLRR on Au film before and after different times of cycling in 2 M HCOOH + 0.1 M $HClO_4$ with scan rate of 0.050 V s^{-1} (same samples as in Figure 5): solid line, control sample without exposure to FAO; dashed lines, samples tested by potential cycling after 30 and 100 h as marked. Ar^+ sputtering rate 0.5 kV min^{-1}.

sample (Figure 6, solid lines) and a sample after 30 h of cycling (Figure 6, dashed lines) suggests significant thinning of the Pt layer. In the latter case, the Au substrate can be detected right from the beginning of a depth-profile characterization. Sputtering deeper into the layers for 5 min reveals more obvious differences in the treated sample manifested by the onset of Pt signal decrease and Au signal increases. At the electrochemically "dead" sample obtained after 100 h of cycling, XPS depth-characterization (Figure 6) suggests insignificant traces of Pt.

Morphological Characterization of Stages of Pt Dissolution. The morphological changes during Pt dissolution pointed out earlier by electrochemical and XPS results have been examined further by SEM and AFM techniques. First it needs to be mentioned that during the course of FAO cycling, that is, Pt dissolution, the shape of the CV changes substantially. Four distinctive CVs obtained on Pt thin films grown by 30 SLRR on Au films are presented in Figure 7 and associated with characteristic points of the decay curve presented already in Figure 3. For the sake of convenience the corresponding decay curve is included in Figure 7 as inset where color coded arrows link accordingly colored CV curves with the decay time line. The most notable CV change that can be observed during cycling besides reduction of the main activity peak is the formation and evolution of a second broad peak in the negative scan at −0.15 V as seen in Figure 7b−d.

This change is accompanied by decrease of the second, more positive peak in the positive potential scan generally associated with oxidative removal of CO_{ad}.[21,45] The observed changes (Figure 7b, blue curve) correspond to the onset of leveling off of the activity decay. Following further cycling the negative scans show a significant magnitude change in the ratio between the sharp current rise at 0.0 V (initially pronounced peak) and the (initially) shoulder that becomes a well-defined peak at −0.15 V with cycling. Along with those changes, a gradual increase of the first and decrease of second peak can further be observed in positive scans (Figure 7c, green curve). Finally, close to the end of testing (Figure 7d, black curve), a single well-defined peak in negative direction at −0.20 V nearly identical in shape and magnitude to the associated oxidation peak can be registered along with complete disappearance of the second most positive oxidation peak.

SEM Characterization. Insight into the surface changes associated with stages depicted in Figure 7 is obtained from corresponding SEM images presented in Figure 8. The SEM micrograph in Figure 8a shows the surface prior to any cycling consistent with our previous work,[28] showing a continuous network of merged Pt clusters and the grain structure of underlying Au films is clearly visible. During FAO cycling, the activity peak shows signs of decay and the surface begins to pit at different spots (image not shown here). The SEM micrograph (Figure 8b) registered just prior to the stage of activity leveling off shows a homogeneously pitted Pt film (dark regions) that has developed a quasi-ordered honeycomb structure. As can be observed in Figure 8c, the latter structure breaks apart and becomes increasingly disorganized at the end of the normalized activity leveling. As the CV curve starts exhibiting negligible hysteresis (Figure 7d) and the normalized activity decays below the 20% mark, most of the Au surface becomes exposed as shown in Figure 8d (some pitting is observed also in the substrate).

The combined analysis of CV curves and SEM images could explain the decay of the activity and loss of Pt due to dissolution. The initial part of activity decay in Figure 7 inset could be associated with dissolution of some roughness (developed in the final stages of Pt growth) leading generally to flattening of the deposit. Then, presumably the surface would behave and dissolve like bulk Pt within the range of relatively steady activity. Although no comparison could be made directly, some analogy can be drawn from a recent work of Komanicky et al.,[61] conducted in 0.6 M $HClO_4$ under constant potential conditions. It has been observed that dissolution of Pt (111) single crystal leaves the surface with

dx.doi.org/10.1021/cs400347u | ACS Catal. 2013, 3, 1709−1718

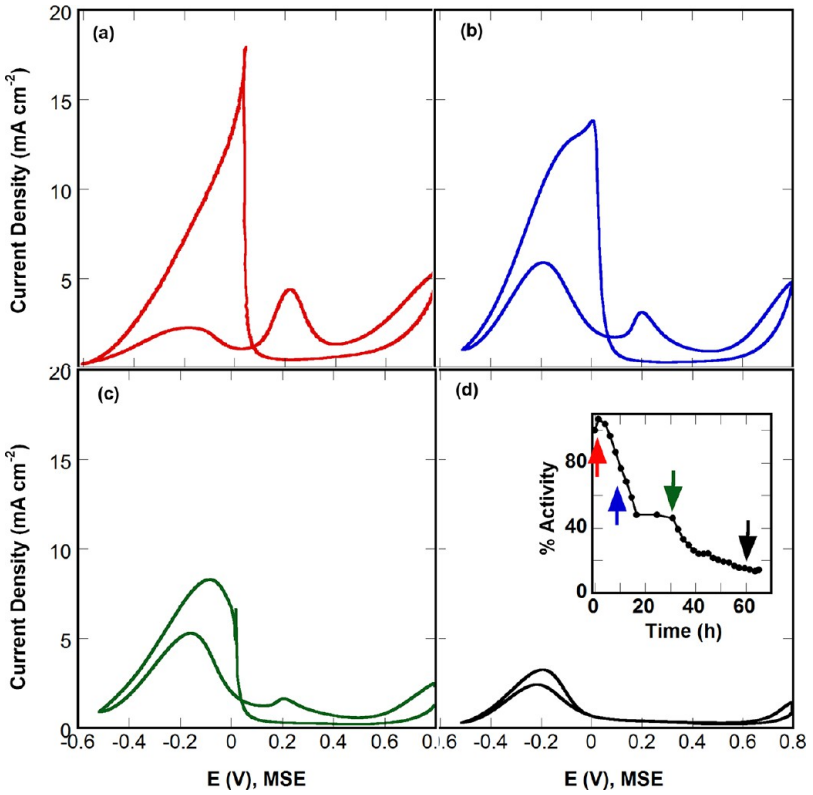

Figure 7. Cyclic voltammetry scans of Pt film deposited on Au-poly by 30 SLRR events using Pb UPD in 2 M HCOOH + 0.1 M $HClO_4$ solution at different times: (a) t = 0 h; (b) t = 10 h; (c) t = 30 h; (d) t = 60 h. Inset, normalized activity decay as a function of time. Scan rate 0.050 V s^{-1}.

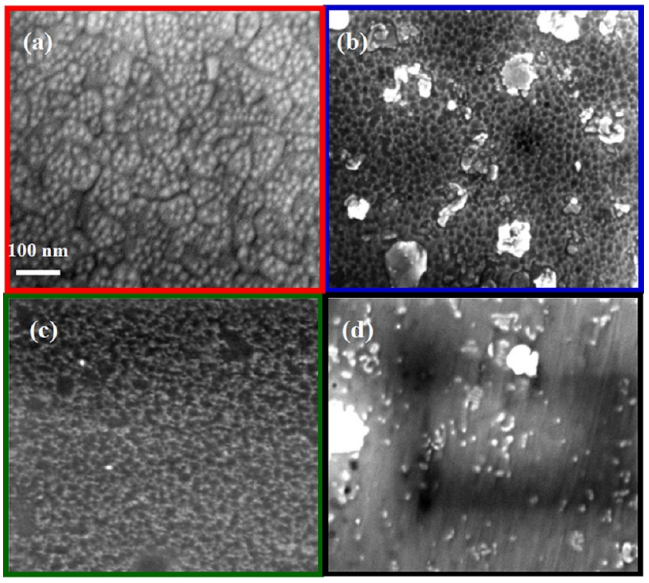

Figure 8. SEM micrographs of Pt film deposited on Au thin films by 30 SLRR events at different stages of dissolution in 2 M HCOOH + 0.1 M $HClO_4$ after (a) 0, (b) 10, (c) 30, and (d) 60 h of cycling with scan rate of 0.050 V s^{-1}.

severe roughening of the step edges as well as the enlargement of preexisting defects leading to the uneven yet uniform thinning of the Pt layer.[61] It is plausible that cycling results in more pronounced roughening, that is, uneven surface dissolution, leading to the emergence of discontinuities and pitting of the Pt layer. As it has been shown in the work of Bauldauf et al.[70] for catalysis on Pd films deposited on Au (*hkl*), the substrate influence becomes significant when a part of it (Au) is exposed to the electrolyte along with the catalyst (Pd). In the present work, the exposure of Au seen in Figure 8b–d leads to a slight shift of the system energetics to more negative potentials manifested by the wide peak formation on the negative scan and its trend with time to reversibility as observed in Figure 7b–d. Along with that, the more positive oxidation peak associated with CO_{ad} oxidation[21,45] decreases steadily suggesting that less CO poisoning takes place with the Au exposure. Finally, as observed in Figure 8d, the Au surface remaining partially covered with Pt clusters behaves electrochemically (Figure 7d) in line with the so-called bifunctional effect reported recently in detail for Pt–Au surfaces in the literature.[27] Moreover the reduction of magnitude of the FAO nearly identical peaks and their shift toward more negative potentials can be correlated with the drastically reduced coverage of Pt on Au.[27]

It must be mentioned that SEM images show undefined 3D clusters scattered over the surface mainly at the lower Pt coverage when the Au surface becomes increasingly exposed. Knowing that XPS results show no Pt at the end of the testing and not seeing such residue in tests run by cycling only in background solution (Figure S1a, Supporting Information), we believe these features are not a result of interaction between Pt and formic acid or biproducts of its oxidation. Although the nature of the features is unknown and the absence of Pt participation warrants no priority for further investigation, we speculate in this work that they are associated with participation of the Au substrate.

AFM Characterization. Further support for the suggested loss of Pt catalyst is obtained by ex situ AFM carried out on Pt films deposited by 10 SLRR events on Au thin films. The AFM

dx.doi.org/10.1021/cs400347u | *ACS Catal.* 2013, 3, 1709–1718

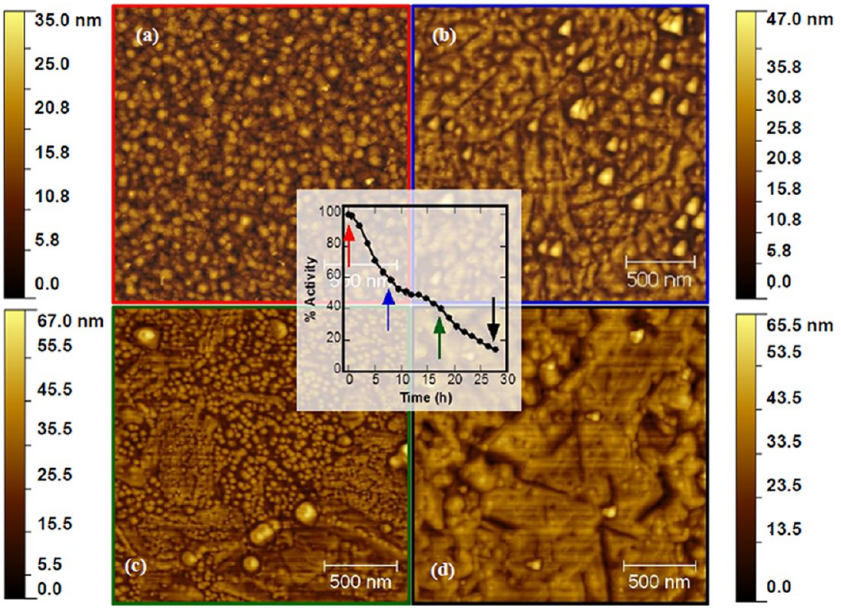

Figure 9. (a) AFM images at different times of cycling of a Pt layer grown on a textured Au(111) film by 10 SLRR events: (a) t = 0 h; (b) t = 8 h; (c) t = 17 h; (d) t = 28 h (catalyst death); (inset) % activity decay of the same film. Solution 2 M HCOOH + 0.1 M $HClO_4$. Scan rate 0.050 V s^{-1}.

study has been conducted on thinner films for the sake of easer experimental control and sample handling that includes shorter time of Pt cycling to reach dissolution stages of interest. AFM imaging was performed right after the samples have been taken out at the stages indicated with color coded arrows on the normalized activity decay plot in the center of Figure 9. The specific stages were chosen in a similar way as those in SEM characterization. The images in Figure 9a–d show the initial surface (a), the catalyst right before (b) and after (c) the activity leveling, and the stage of complete Pt dissolution (d). The AFM image of the untreated sample, Figure 9a, reveals Pt layer morphology that is consistent with the one seen in our previous work.[28] As the dissolution process progresses, the uniform Pt surface undergoes changes revealing (i) contours of major morphological features of the underlying substrate such as grain boundaries and edges (manifested by "grooving" lines) and (ii) hints of structuring with formation of larger clusters surrounded by smaller Pt clusters between them (Figure 9b). More detailed dimensional analysis of holes surrounded by six clusters suggests close similarity with the length scale of the honeycomb cells in Figure 8b. However, despite the general similarity, Figure 9b depicts a slightly earlier stage of testing than the one presented by Figure 8b. Support for this statement can be seen in SEM micrograph in Figure 10, which represents the surface after 5h of cycling. The formation of isolated holes in the continuous Pt film can be clearly observed. Proceeding further with the analysis of Figure 9c presenting a catalyst taken out at the onset of the second activity decay (green arrow), one sees substantial discontinuity of the layer consisting of more or less isolated Pt clusters. This structure is similar yet more discontinuous to the broken honeycomb structure seen by SEM in Figure 8c. Apparently, the Pt dissolution process in that case has advanced to the point of revealing (lower right portion) parts of bare Au surface. Another interesting similarity between the AFM and SEM experiments is associated with the bigger cluster formations seen in Figure 9b,c that could be associated by size and shape with the 3D clusters seen on the SEM micrographs with the progress of the experiment. Finally, Figure 9d obtained on a catalyst reaching the final stage of

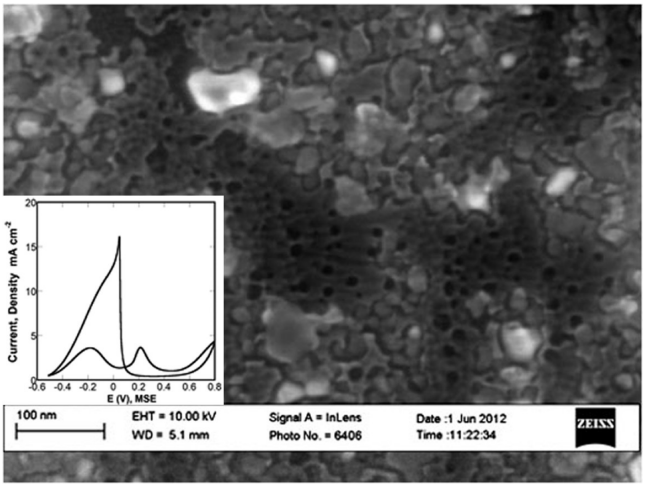

Figure 10. SEM micrograph of Pt film deposited on Au-poly by 30 SLRR events after 5 h of cycling in 2 M HCOOH + 0.1 M $HClO_4$ with scan rate of 0.050 V s^{-1}. Inset shows a characteristic CV obtained prior to the SEM imaging.

activity loss depicts mainly Au surface sporadically covered by isolated Pt clusters. Closer examination of the same image reveals characteristic for the Au (111) faceted triangular terraces separated by step regions. Also, some of the white spots could still be seen on the surface, but more importantly one sees enough evidence for pitting of the Au substrate itself at the end of the process. A comparison could be made also between the surface in Figure 9d and an AFM image of bare Au thin film at identical magnification. It could be seen in Figure 11 that the overall macrostructure of the post-treated Au substrate differs from the untreated one only in minor details like local corrugations and pits, whereas the macrostructure in both cases remains nearly identical. This is not unexpected when accounting for the Au dissolution seen in our experiments and elsewhere in the literature[56] to generate minor to moderate microstructural damages in the absence of formic acid (Figure S1, Supporting Information). In summary, both AFM and SEM

dx.doi.org/10.1021/cs400347u | ACS Catal. 2013, 3, 1709–1718

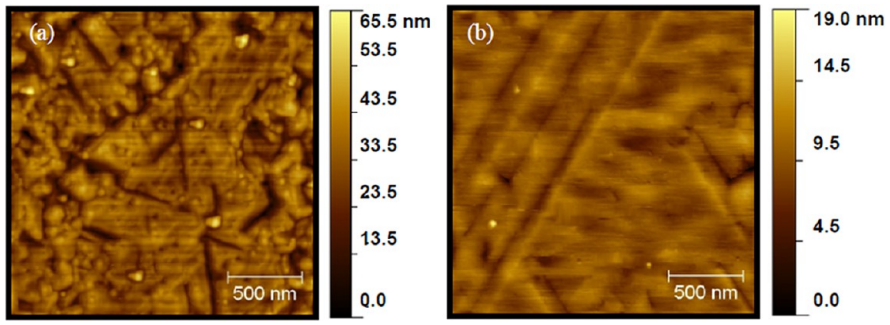

Figure 11. AFM images comparing (a) Pt/Au (thin film) after the end of long-term cycling (about 50 h) in the potential range of −0.500 to +0.800 V (MSE) with sweep rate of 0.050 V s^{-1} in 0.1 M $HClO_4$ and (b) bare Au(thin film) surface.

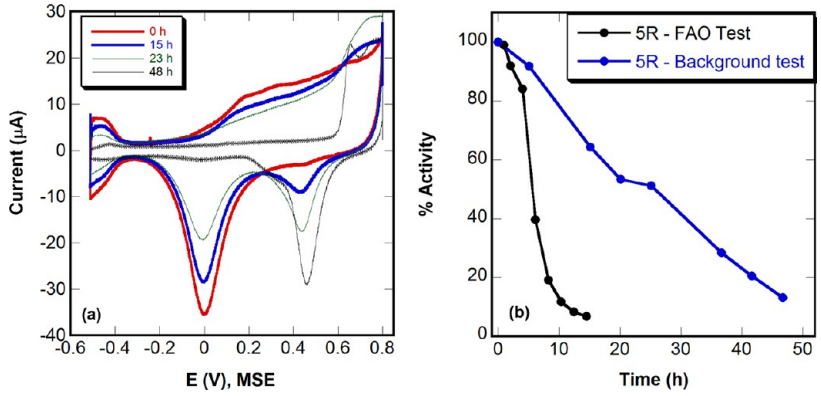

Figure 12. (a) Cyclic voltammetries in 0.1 M $HClO_4$ solution at different times of Pt film deposited on Au-poly by 5 SLRR events, scan rate 0.050 V s^{-1}. (b) Normalized activity decay for the same film (blue) compared with the one cycled in the presence of HCOOH (black).

characterization results demonstrate a common general trend in morphological evolution during dissolution regardless of the Pt layer thickness. Both experiments also associate well characteristic points in the activity decay curve with specific structure and morphology of the dissolving Pt layer. This along with the precise thickness control enabled by the SLRR approach for growing Pt is of great importance for quantifying the rate of Pt dissolution during FAO.

Quantitative Analysis of the Pt Dissolution Rate. Many groups over the years have used different means to quantify the dissolution of Pt.[51,56−59,61] Johnson et al.[51] measured Pt dissolution charge density of 4.7 $\mu C \cdot cm^{-2} \cdot cycle^{-1}$ in 1 M H_2SO_4 and 3.5 $\mu C \cdot cm^{-2} \cdot cycle^{-1}$ in 0.1 M $HClO_4$ acid during potential cycling between −0.2 and +0.8 V (MSE) with the rate of 0.5 V min^{-1}. Taking in consideration a length of cycle of 240 s (~15 cycles per hour) and assuming for the sake of simplicity (111) crystallographic orientation of the dissolving Pt surface and only Pt(II) complex as dissolution product, one can make conversion of the charge density per cycle to mass density per hour. Thus, such consideration associates 1 μC with 1.02 ng of Pt resulting in Pt dissolution rate of 71.9 $ng \cdot cm^{-2} \cdot h^{-1}$ in H_2SO_4 and 53.6 $ng \cdot cm^{-2} \cdot h^{-1}$ in $HClO_4$. The results of Johnson et al.[51] could not be directly compared with the results of our work because of differences in the sweep rates. However, one can still justify a coarse comparison based on practically identical positive potential limit (+0.8 V in both cases) and close overall potential range (1.3 V in our case vs 1.0 V in Johnson's work[51]). Relying on this justification, we present in this section an estimate of the average dissolution rate made by considering the total time for complete depletion of Pt in films of three different thicknesses (5*R*, 15*R*, and 30*R*) presented, tested, and characterized in this work. For the sake of simplicity, we have considered in the estimate 100% efficient Pt deposition (based on earlier EQCM results showing practically 1 ML of Pt deposited per SLRR event[28]), (111) crystallographic orientation for all Pt films (470 ng per ML), and virtually complete depletion of Pt at the 20% activity level, that is, of negligible amount of catalyst left (supported by SEM and AFM results shown earlier). Based upon the measured durability of Pt films with three different thicknesses, the average rate of Pt dissolution was determined to be 3.9 ± 0.5 $ng \cdot cm^{-2} \cdot cycle^{-1}$ and 272 ± 30 $ng \cdot cm^{-2} \cdot h^{-1}$ revealing 4−5-fold faster kinetics in the presence of formic acid compared with Johnson's[51] dissolution rates in perchloric acid only.

Taking a further comparative step, we performed experiments in the absence of formic acid by subjecting a Pt film grown by 5 replacements to identical cycling conditions in perchloric acid only as shown in Figure 12. It can be clearly seen in Figure 12a that in the absence of formic acid, the only observed phenomena are the reduction/formation of Pt oxide coupled with partial formation/stripping of the H UPD layer on the Pt film. After approximately 5 h, the Au oxide peak starts to appear at a potential of 0.460 V indicating dissolution of the Pt surface. As the film is cycled, the ratio of the peaks starts to increase in favor of the Au owing to further exposure of Au surface to the solution. With the progress of Pt dissolution, the ratio becomes about 1:1 at approximately 23 h. After 35 h (not shown), the Pt oxide peak is much smaller as surface is largely dominated by Au, and at 48 h, no presence of Pt is registered and only Au redox behavior is seen. Along with the dissolution, the film was tested in separate cell for FAO activity in order to collect information for performing a quantitative determination

dx.doi.org/10.1021/cs400347u | *ACS Catal.* 2013, 3, 1709−1718

of the rate of activity decay following the routines of the present work (results shown in Figure S2, Supporting Information). The activity decay along with the corresponding one (taken for comparison from Figure 4) in the presence of formic acid is shown in Figure 12b. It is clear that in the absence of formic acid, the rate of dissolution is about 5 times slower as the film under FAO reaches 20% activity at 8 h compared with the film cycled in perchlorate, which reaches the same activity at about 42 h. This difference relates to a slower Pt dissolution rate of approximately 0.9 ± 0.1 ng·cm^{-2}·cycle^{-1} and 61 ± 8 ng·cm^{-2}·h^{-1} measured in perchlorate solution. The comparison of results on Pt dissolution rates in the presence and absence of formic acid undoubtedly confirms the significant difference of Pt dissolution rates. In addition, our data validates the proposed herein approach for assessing Pt dissolution kinetics given the remarkable agreement with the work of Johnson et al.[51] and the comparability with realm of results on Pt dissolution obtained recently by Mayrhofer et al[55] by ICP-MS in perchloric acid solution.

Overall, the reason for such dramatic difference in Pt dissolution rates is unclear in the absence of understanding of the mechanism of Pt dissolution in FAO. At the same time, this difference is in concert with our previous work where Pt nanoparticle catalysts with low FAO activity were found to dissolve considerably slower than ultrathin film catalysts containing the same amount of Pt and featuring higher activity.[43] The trend similarity in both cases implies that the rate of Pt dissolution is somehow proportional to or dependent on the overall oxidation, positive charge, Q^{ox}, accumulated per cycle (i.e., $Q^{ox}_{\text{thin-film-FAO}} > Q^{ox}_{\text{nanoparticle-FAO}} > Q^{ox}_{\text{background}}$). This observation is unexpected because Pt, as catalyst, should remain unaffected by the catalyzed process. Thus, the higher overall oxidation charge would be solely contributed by the different rate of FAO. All that would lead eventually to a constant rate of Pt dissolution. Therefore, the charge-dependent dissolution rate observed experimentally in our work implies indirectly that the formic acid contributes in a certain way to the loss of Pt in the course of potential cycling. Apparently, the nature of this contribution is unclear, and more fundamental studies are needed for understanding quantitatively the difference in Pt dissolution in the absence and presence of formic acid. Such studies should focus on the role of Pt in the oxidation of CO and other intermediates (i.e., CO, $HCOO^-$, COH^{3-})[22,36] during a potential cycle of FAO testing.[22] Experimentally, the emphasis would be on the delicate balance between CO/intermediate adsorption and Pt oxidation/reduction that could realistically be tested by (i) cycling with different scan rates, (ii) varying the positive potential limit, and (iii) even performing potentiostatic experiments at different potentials where both phenomena are enabled. Obtaining quantitative information of these experiments would allow one to not only ascertain the governing role of CO poisoning and Pt dissolution to the durability of Pt catalysts for FAO but also derive details on the specific contribution of adsorption, intermediate oxidation, and Pt redox cycle to the catalyst's lifetime.

CONCLUSIONS

Electrochemical approaches are used to demonstrate Pt dissolution at a detectable rate in FAO during cycling in a potential range limited by the onset of Pt oxidation. The Pt loss has been confirmed quantitatively by surface and depth-profile XPS characterization. In addition, when subjected to FAO, Pt thin films of different thicknesses deposited on Au by up to 30 SLRR events of Pb UPD (~10 nm thickness) have shown gradual decay of the normalized activity featuring plateaus at about 45−55% value. The plateau duration and the catalyst lifetime have been correlated with the Pt layer thickness. Distinct changes in the CV behavior in the course of activity decay have been associated with characteristic morphological changes registered in SEM and AFM characterization at different stages of the Pt dissolution process. Formation of Au exposed regions has been shown to coincide with the formation of a new oxidation wave at more negative potentials accompanied by a decrease of the positive peak attributed to oxidative removal of CO_{ad}. A formation of a uniform 2D Pt network degrading to scarce Pt remnants at the end of catalyst life has been associated with a CV curve showing nearly identical anodic and cathodic behavior. The quantitative aspect of this study is supported by measuring the Pt dissolution rate that has been found to be 3.9 ± 0.5 ng·cm^{-2}·cycle^{-1} and 272 ± 30 ng·cm^{-2}·h^{-1} in FAO testing environment and 0.9 ± 0.1 ng·cm^{-2}·cycle^{-1} and 61 ± 8 ng·cm^{-2}·h^{-1} in the absence of formic acid (in background solution only). The reported measurements are performed by a new method utilizing the precise control of amount deposited Pt provided by the SLRR approach along with a detailed knowledge on the kinetics of Pt corrosion in the Pt/Au system. The results obtained in this work are in a good agreement with literature data for Pt dissolution in background electrolyte. Future work is planned on studying in detail the mechanism of Pt dissolution in the presence of formic acid.

ASSOCIATED CONTENT

Supporting Information

Additional characterization results on experiments carried out with Pt films in background electrolyte. This material is available free of charge via the Internet at http://pubs.acs.org.

AUTHOR INFORMATION

Corresponding Author

*E-mail: dimitrov@binghamton.edu. Tel: +1 (607) 777-4271. E-mail: N.Vasiljevic@bristol.ac.uk. Tel: +44 (117) 331-7739.

Notes

The authors declare no competing financial interest.

ACKNOWLEDGMENTS

M.F. and N.D. acknowledge the financial support of the National Science Foundation, Division of Materials Research (Grant DMR-0742016). J.N. and N.V. acknowledge the support of the Bristol Centre for Nanoscience and Quantum Information, University of Bristol, U.K. J.N. is grateful for the postgraduate Royal Thai Government Scholarship.

REFERENCES

(1) Debe, M. K. *Nature* **2012**, *486*, 43−51.
(2) Pickup, P. G.; Yu, X. *J. Power Sources* **2008**, *182*, 124−132.
(3) Arico, A. S.; Bruce, P.; Scrosati, B.; Tarascon, J.-M.; Schalkwijk, W. V. *Nat. Mater.* **2005**, *4*, 366−377.
(4) Adzic, R. R. *Recent Advances in the Kinetics of Oxygen Reduction*; Wiley-VCH, Inc: New York, 1998.
(5) Shao, M. H.; Huang, T.; Liu, P.; Zhang, J.; Sasaki, K.; Vukmirovic, M. B.; Adzic, R. R. *Langmuir* **2006**, *22*, 10409−10415.
(6) Stamenkovic, V. R.; Fowler, B.; Mun, B. S.; Wang, G.; Ross, P. N.; Lucas, C. A.; Markovic, N. M. *Science* **2007**, *315*, 493−497.
(7) Nilekar, A. U.; Xu, Y.; Zhang, J. L.; Vukmirovic, M. B.; Sasaki, K.; Adzic, R. R.; Mavrikakis, M. *Top. Catal.* **2007**, *46*, 276−284.

(8) Koenigsmann, C.; Zhou, W. P.; Adzic, R. R.; Sutter, E.; Wong, S. S. *Nano Lett* **2010**, *10*, 2806−2811.
(9) Markovic, N. M.; Gasteiger, H. A., Jr.; P. N. R.; Jiange, X.; Villegas, I.; Weaver, M. J. *Electrochim. Acta* **1995**, *40*, 91−98.
(10) Ross, P. N. *The Science of Electrocatalysis on Bimetallic Surfaces*; Wiley-VCH: New York, 1998.
(11) Adzic, R. R.; Zhang, J.; Sasaki, K.; Vukmirovic, M. B.; Shao, M.; Wang, J. X.; Nilekar, A. U.; Mavrikakis, M.; Valerio, J. A.; Uribe, F. *Top. Catal.* **2007**, *46*, 249−262.
(12) Arenz, M.; Stamenkovic, V.; Schmidt, T. J.; Wandelt, K.; Ross, P. N.; Markovic, N. M. *Phys. Chem. Chem. Phys.* **2003**, *5*, 4242.
(13) Choi, J.-H.; Jeong, K.-J.; Dong, Y.; Han, J.; Lim, T.-H.; Lee, J.-S.; Sung, Y.-E. *J Power Sorces* **2006**, *163*, 71−75.
(14) Zhang, L. J.; Wang, Z. Y.; Xia, D. G. *J. Alloys Compd.* **2006**, *426*, 268−271.
(15) Tripković, A. V.; Popović, K. D.; Stevanović, R. M.; Socha, R.; Kowal, A. *Electrochem. Commun.* **2006**, *8*, 1492−1498.
(16) Xu, D.; Bliznakov, S.; Liu, Z.; Fang, J.; Dimitrov, N. *Angew. Chem., Int. Ed.* **2010**, *49*, 1282−1285.
(17) Yang, H.; Dai, L.; Xu, D.; Fang, J.; Zou, S. *Electrochim. Acta* **2010**, *55*, 8000−8004.
(18) Hwang, S.-M.; Bonevich, J. E.; Kim, J. J.; Moffat, T. P. *J. Electrochem. Soc.* **2011**, *158*, B1019.
(19) De-los-Santos-Alvarez, N.; Alden, L. R.; E., R.; Wang, F. J.; DiSalvo, F. J.; Abruna, H. D. *J. Electroanal. Chem.* **2009**, *626*, 14−22.
(20) Rice, C.; Ha, S.; Masel, R. I.; Waszczuk, P.; Wieckowski, A.; Barnard, T. *J. Power Sources* **2002**, *111*, 83−89.
(21) Capon, A.; Parsons, R. *J. Electroanal. Chem.* **1973**, *44*, 239−254.
(22) Capon, A.; Parsons, R. *J. Electroanal. Chem.* **1973**, *45*, 205−231.
(23) Capon, A.; Parsons, R. *J. Electroanal. Chem.* **1973**, *44*, 1−7.
(24) Parsons, R.; Vandernoot, T. *J. Electroanal. Chem.* **1988**, *257*, 9−45.
(25) Sun, S. G.; Clavilier, J.; Bewick, A. *J. Electroanal. Chem.* **1988**, *240*, 147−159.
(26) Chang, S.-C.; Leung, L.-W. H.; Weaver, M. J. *J. Phys. Chem.* **1990**, *94*, 6013−6021.
(27) Obradovic, M. D.; Tripkovic, A. V.; Gojkovic, S. L. *Electrochim. Acta* **2009**, *55*, 204−209.
(28) Fayette, M.; Liu, Y.; Bertrand, D.; Nutariya, J.; Vasiljevic, N.; Dimitrov, N. *Langmuir* **2011**, *27*, 5650−5658.
(29) Brankovic, S. R.; McBreen, J.; Adzic, R. R. *J. Electroanal. Chem.* **2001**, *503*, 99−104.
(30) Hwang, S. M.; Bonevich, J. E.; Kim, J. J.; Moffat, T. P. *J. Electrochem. Soc.* **2011**, *158*, B1019−B1028.
(31) Liu, Y.; Abe, H.; Edvenson, H. M.; Ghosh, T.; DiSalvo, F. J.; Abruna, H. D. *Phys. Chem. Chem. Phys.* **2010**, *12*, 12978−12986.
(32) Neurock, M.; Janik, M.; Wieckowski, A. *Faraday Discuss.* **2009**, *140*, 363−378.
(33) Samjeske, G.; Miki, A.; Ye, S.; Yamakata, A.; Mukouyama, Y.; Okamoto, H.; Osawa, M. *J. Phys. Chem. B* **2005**, *109*, 23509−23516.
(34) Chen, Y.-X.; Heinen, M.; Jusys, Z.; Behm, R. J. *Chem. Phys. Chem.* **2007**, *8*, 380−385.
(35) Gao, W.; Keith, J. A.; Anton, J.; Jacob, T. *J. Am. Chem. Soc.* **2010**, *132*, 18377−18385.
(36) Cuesta, A.; Cabello, G.; Gutierrez, C.; Osawa, M. *Phys. Chem. Chem. Phys.* **2011**, *13*, 20091−20095.
(37) Mukouyama, Y.; Kikuchi, M.; Samjeske, G.; Osawa, M.; Okamoto, H. *J. Phys. Chem. B* **2006**, *110*, 11912−11917.
(38) Chen, Y. X.; Heinen, M.; Jusys, Z.; Behm, R. J. *Langmuir* **2006**, *22*, 10399−10408.
(39) Chen, Y. X.; Ye, S.; Heinen, M.; Jusys, Z.; Osawa, M.; Behm, R. J. *J. Phys. Chem. B* **2006**, *110*, 9534−9544.
(40) Chen, Y. X.; Heinen, M.; Jusys, Z.; Behm, R. J. *Angew. Chem., Int. Ed.* **2006**, *45*, 981−985.
(41) Grozovski, V.; Climent, V.; Herrero, E.; Feliu, J. M. *Phys. Chem. Chem. Phys.* **2010**, *12*, 8822−8831.
(42) McCurry, D. A.; Kamundi, M.; Fayette, M.; Wafula, F.; Dimitrov, N. *ACS Appl. Mater. Interfaces* **2011**, *3*, 4459−4468.
(43) Bromberg, L.; Fayette, M.; Martens, B.; Luo, Z. P.; Wang, Y.; Xu, D.; Zhang, J.; Fang, J.; Dimitrov, N. *Electrocatalysis* **2012**, 1−13.
(44) Borup, R.; Meyers, J.; Pivovar, B.; Kim, Y.; Mukundan, R.; Garland, N.; Myers, D.; Wilson, M.; Garzon, F.; Wood, D.; Zelenay, P.; More, K.; Stroh, K.; Zawodzinski, T.; Boncella, J.; McGrath, J. E.; Inaba, M.; Miyatake, K.; Hori, M.; Ota, K.; Ogumi, Z.; Miyata, S.; Nishikata, A.; Siroma, Z.; Uchimoto, Y.; Yasuda, K.; Kimijima, K.-i.; Iwashita, N. *Chem. Rev.* **2007**, *107*, 3904−3951.
(45) Tian, M.; Conway, B. E. *J. Electroanal. Chem.* **2008**, *616*, 45−56.
(46) Shao, Y.; Yin, G.; Gao, Y. *J. Power Sources* **2007**, *171*, 558−566.
(47) Sasaki, K.; Shao, M.; Adzic, R. R. *Dissolution and Stabilization of Platinum in Oxygen Cathodes*; Springer Science + Business Media, LLC: New York, 2009.
(48) Shao-Horn, Y.; Sheng, W. C.; Chen, S.; Ferreira, P. J.; Holby, E. F.; Morgan, D. *Top. Catal.* **2007**, *46*, 285−305.
(49) Hiraoka, F.; Matsuzawa, K.; Shigenori, M. *Electrocatalysis* **2013**, *4*, 10−16.
(50) Carlton, C. E.; Chen, S.; Ferreira, P. J.; Allard, L. F.; Shao-Horn, Y. *J. Phys. Chem. Lett.* **2012**, *3*, 161−166.
(51) Johnson, D. C.; Napp, D. T.; Bruckenstein, S. *Electrochim. Acta* **1970**, *15*, 1493−1509.
(52) Mitsushima, S.; Koizumi, Y.; Uzuka, S.; Ota, K.-I. *Electrochim. Acta* **2008**, *54*, 455−460.
(53) Inzelt, G.; Berkes, B.; Kriston, A. *Electrochim. Acta* **2010**, *55*, 4742−4749.
(54) Rinaldo, S. G.; Stumper, J.; Eikerling, M. *J. Phys. Chem. C* **2010**, *114*, 5773−5785.
(55) Topalov, A. A.; Koatsounaros, I.; Auinger, M.; Cherevko, S.; Meier, J. C.; Klemm, S. O.; Mayrhofer, K. J. *Angew. Chem., Int. Ed.* **2012**, *51*, 12613−12615.
(56) Rand, D. A. J.; Woods, R. *J. Electroanal. Chem.* **1972**, *35*, 209−218.
(57) Kinoshita, K.; Lundquist, J. T.; Stonehart, P. *J. Electroanal. Chem.* **1973**, *48*, 157−166.
(58) Wang, X.; Kumar, R.; Myers, D. J. *Electrochem. Solid-State Lett.* **2006**, *9*, A225.
(59) Ofstad, A. B.; Thomassen, M. S.; Gomez de la Fuente, J. L.; Seland, F.; Møller-Holst, S.; Sunde, S. *J. Electrochem. Soc.* **2010**, *157*, B621.
(60) Ota, K.; Nishigori, S.; Kamiya, N. *J. Electroanal. Chem.* **1988**, *257*, 205−215.
(61) Komanicky, V.; Chang, K. C.; Menzel, A.; Markovic, N. M.; You, H.; Wang, X.; Myers, D. *J. Electrochem. Soc.* **2006**, *153*, B446.
(62) Zhang, X.; Galindo, H. M.; Garces, H. F.; Baker, P.; Wang, X.; Pasaogullari, U.; Suib, S. L.; Molter, T. *J. Electrochem. Soc.* **2010**, *157*, B409.
(63) Lipkowski, J.; Shi, Z.; Chen, A.; Pettinger, B.; Bilger, C. *Electrochim. Acta* **1988**, *43*, 2875−2888.
(64) Dios, F. J. G. d.; Gomez, R.; Feliu, J. M. *Langmuir* **2005**, *21*, 7439−7448.
(65) Liu, Y.; Bliznakov, S.; Dimitrov, N. *J. Phys. Chem. C* **2009**, *113*, 12362−12372.
(66) Strmcnik, D.; Tripkovic, D.; van der Vliet, D.; Stamenkovic, V.; Marković, N. M. *Electrochem. Commun.* **2008**, *10*, 1602−1605.
(67) Chen, Q.-S.; Solla-Gullón, J.; Sun, S.-G.; Feliu, J. M. *Electrochim. Acta* **2010**, *55*, 7982−7994.
(68) Rincon, A.; Perez, M. C.; Gutierrez, C. *Electrochim. Acta* **2010**, *55*, 3152−3156.
(69) Prieto, M. J.; Filho, U. P. R.; Landers, R.; Tremiliosi-Filho, G. *Phys. Chem. Chem. Phys.* **2012**, *14*, 599−606.
(70) Baldauf, M.; Kolb, D. M. *J. Phys. Chem.* **1996**, *100*, 11375−11381.